Magnitude of Sarcomere Extension Correlates with Initial Sarcomere Length during Lengthening of Activated Single Fibers from Soleus Muscle of Rats

Appaji Panchangam,* Dennis R. Claflin,† Mark L. Palmer,*‡ and John A. Faulkner*§
*Department of Biomedical Engineering, †Department of Surgery, Section of Plastic Surgery, ‡Division of Kinesiology, and §Department of Molecular and Integrative Physiology, University of Michigan, Ann Arbor, Michigan

ABSTRACT A laser-diffraction technique was developed that rapidly reports the lengths of sarcomeres (L_s) in serially connected sectors of permeabilized single fibers. The apparatus translates a laser beam along the entire length of a fiber segment within 2 ms, with brief stops at each of 20 contiguous sectors. We tested the hypothesis that during lengthening contractions, when maximally activated fibers are stretched, sectors that contain the longer sarcomeres undergo greater increases in L_s than those containing shorter sarcomeres. Fibers ($n = 16$) were obtained from the soleus muscles of adult male rats and the middle portions (length = 1.05 ± 0.11 mm; mean ± SD) were investigated. Single stretches of strain 27% and a strain rate of 54% s^{-1} were initiated at maximum isometric stress and resulted in a 19 ± 9% loss in isometric stress. The data on L_s revealed that 1), the stretch was not distributed uniformly among the sectors, and 2), during the stretch, sectors at long L_s before the stretch elongated more than those at short lengths. The findings support the hypothesis that during stretches of maximally activated skeletal muscles, sarcomeres at longer lengths are more susceptible to damage by excessive strain.

INTRODUCTION

Skeletal muscle is routinely subjected to three types of contractions: shortening, isometric (fixed-length), and lengthening (1). Of the three, only lengthening contractions are capable of producing muscle injury (2). Structural damage to muscle fibers is evident by electron microscopy immediately after stretches of maximally activated whole muscle groups (3–5), whole muscles (6–8), intact single fibers (9), and permeabilized single fibers (10). In each case the damage is localized within single sarcomeres or small groups of sarcomeres that appear to be distributed randomly among the intact sarcomeres. The extent of the injury produced by a lengthening contraction of whole muscles (7,11,12) and segments of permeabilized single fibers (10) is affected by a combination of mechanical factors that include the initial length, the strain, the stress during the stretch, and the work done during the stretch.

Although the gross mechanical factors that lead to injury have been identified, the underlying causative factors and events have been described only through a theoretical model (13). The model supports the premise that the injury is due to nonuniformity in sarcomere lengths (L_s) and predicts that during a lengthening contraction, some sarcomeres at longer lengths are stretched beyond filament overlap, whereas shorter sarcomeres are strained but maintain filament overlap. The underlying causes of the nonuniformity in L_s are complex (14). Telley and Denoth (15) concluded that a major cause is the biological variability in the strength of opposing half-sarcomeres that is due to intrinsic differences in the number of potential force-generating cross-bridges in the two halves. Although nonuniformity in L_s has been implicated as the leading cause of excessive stretch and subsequent damage to localized groups of sarcomeres during lengthening contractions (7–10), this hypothesis has not been supported by definitive evidence. Furthermore, direct imaging of single myofibrils (16) has challenged the concept that a loss of thick and thin filament overlap, as in ''sarcomere popping'' (13), of some sarcomeres explains the condition of contraction-induced injury.

Macpherson et al. (17) used laser diffraction to measure L_s sequentially in five discrete locations along a permeabilized single fiber. They demonstrated that regions of an activated fiber that contained the longest sarcomeres before the stretch showed the highest number of overstretched and disrupted sarcomeres as observed in electron micrographs obtained after the fibers were returned to their original length. The finding is consistent with the hypothesis that sarcomere length is variable and sarcomeres at longer lengths are more susceptible to injury. They also reported that, after the activated fibers were returned to original length after the stretch, the sarcomeres in the injured regions appeared to be longer than they were before the stretch. Since they did not measure L_s of the activated fibers at the peak of the stretch, whether the L_s before the stretch had any influence on the strain of a region during the stretch is not clear. The purpose of our investigation was to test the hypothesis that during lengthening of maximally activated permeabilized fibers, regions that contain longer sarcomeres during the preceding isometric activation period undergo more stretch than regions that contain shorter sarcomeres. A rigorous test of this hypothesis requires simultaneous measurement of the lengths of each of the serially connected groups of sarcomeres during

Submitted July 24, 2007, and accepted for publication April 16, 2008.

Address reprint requests to John A. Faulkner, Room 2035, BSRB, University of Michigan, 109 Zina Pitcher, Ann Arbor, MI 48109-2200. Tel.: 734-764-4378; Fax: 734-615-3292; E-mail: jafaulk@umich.edu.

Editor: K. W. Ranatunga.

0006-3495/08/08/1890/12 $2.00

doi: 10.1529/biophysj.107.118109

stretches of activated fibers. We developed a technique that approximates this ideal by measuring, within a 2-ms time period, the L_s of each of 20 contiguous sectors that span the entire length of the fiber segment.

MATERIALS AND METHODS

Permeabilized single fiber preparation

Adult male rats (Fisher 344; $n = 5$; age = 6–10 months) were anesthetized with an intraperitoneal injection of sodium pentobarbitone (50 mg kg^{-1}), with supplemental doses administered as needed to prevent response to tactile stimuli. The soleus muscle was exposed and the proximal and distal tendons were isolated. The tendons were cut and the muscle removed from the hind limb. Muscles were placed immediately into cold (~4°C) skinning solution (see Solutions below). After the soleus muscles were removed from both legs, the rats were euthanized with an overdose of sodium pentobarbitone (100 mg kg^{-1}) and a bilateral pneumothorax procedure was performed. All experimental procedures were approved by the University of Michigan Committee on the Use and Care of Animals and in accordance with the Guide for the Care and Use of Laboratory Animals (Department of Health and Human Services publication No. 85–23 (National Institutes of Health), revised 1985, Office of Science and Health Reports, Bethesda, MD). Bundles of fibers ~5 mm in length and 1–2 mm in diameter were dissected from the soleus muscles. After dissection, the bundles were immersed for 30 min in skinning solution to which the nonionic detergent Brij 58 was added (0.5% w/v). Fiber bundles were subsequently placed in storage solution and maintained for 24 h at 4°C before being stored at −20°C for periods of up to 4 months.

To begin an experiment, a bundle of fibers was removed from the storage solution and placed in relaxing solution for 25 min at 4°C. Permeabilized single fiber segments (''fibers'') were then pulled from the bundle using fine forceps with the aid of a dissecting microscope and dark-field illumination. Isolated fibers were transferred to a fluid exchange bath (volume = 330 μl) containing relaxing solution maintained at 15°C using feedback-controlled Peltier devices (Fig. 1). One end of the fiber was secured to a force transducer (model 403A; Aurora Scientific) using two ties of 10-0 monofilament nylon suture. The other end was attached in the same manner to the lever arm of a servomotor (model 322C; Aurora Scientific, Aurora, Canada). The points of attachment of the fiber to the force transducer and servomotor were short lengths of 29-gauge stainless-steel thin-wall tubing (outer diameter = 330 μm) that had been fastened with epoxy to the respective instruments. A typical preparation is shown in Fig. 1 *B* with only two of the four sutures visible within the image frame. The approximate resting L_s was determined by projecting the laser diffraction pattern produced by the middle section of the fiber onto a calibrated target screen. The fiber length was then adjusted to obtain the desired L_s by translating the servomotor using a micrometer drive. Fiber length (L_f) was defined as the distance between the innermost ties when the mean L_s was 2.5 μm (Fig. 1 *B*). The length of the fiber being probed optically (L_{op}) was obtained by measuring the distance between the ends of the stainless-steel tubing to which the fiber was attached and then subtracting the width of the laser spot (Fig. 1 *B*). The cross-sectional area (CSA) of the fibers was measured as described later in this section and the force measurements were normalized by the CSA to obtain stress (kN m^{-2}). During a maximum isometric activation, the diffraction pattern produced by a fiber was inspected visually. A fiber was rejected if the diffraction pattern was faint or diffuse. At the end of an experiment, any fiber that had gross markers of damage, such as tears, or other disruptions was also rejected. Six of 22 fibers were rejected on the basis of these criteria.

Fiber activation

The content of the bath was controlled using a fluid exchange system. Fluid from the bath was emptied in ~700 ms by opening a solenoid valve to a vacuum line. After a brief pause of ~500 ms, during which the fiber was suspended in air, fresh solution was delivered by a syringe pump at the rate of 0.3 ml s^{-1} via multiple conduits near the floor of the chamber. Fresh fluid thus entered the chamber from the bottom, with the liquid-air interface forming a plane parallel to the long axis of the fiber and rising rapidly to meet the fiber. Based on the dimensions of the chamber, the fiber diameter, and the fluid exchange rate, we estimated that the elapsed time between the first contact of the fiber with the rising liquid and its complete submersion was

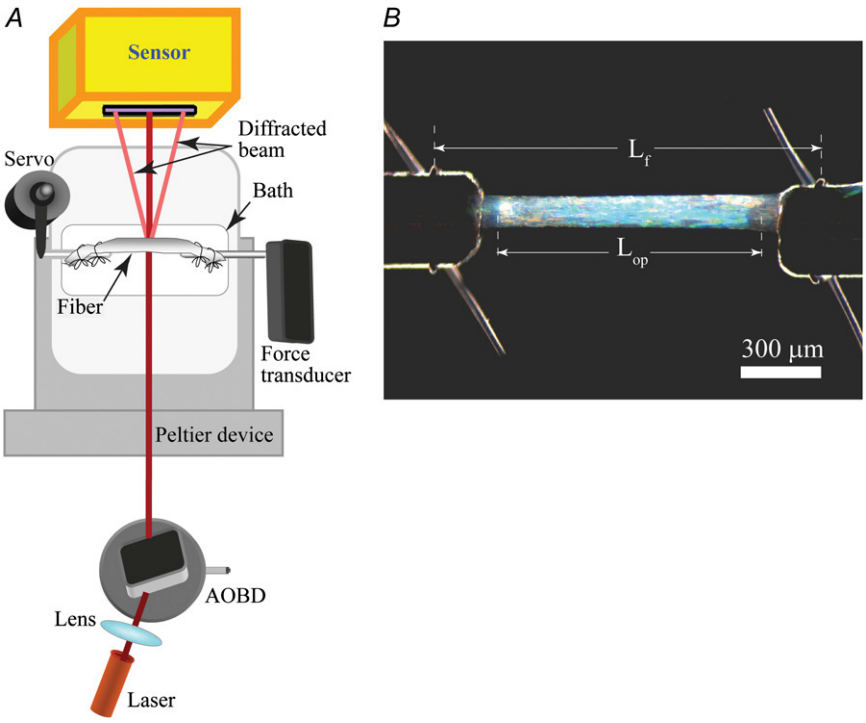

FIGURE 1 (*A*) Schematic diagram of the experimental apparatus. (*B*) Top view of a sample fiber (under dark-field illumination) mounted in the bath showing only the two innermost ties. The force-producing length (L_f) and the investigation length (L_{op}) were measured as indicated in the figure with the L_s of a central section adjusted to ~2.5 μm.

~50 ms. Relaxed single fibers were activated after they were first equilibrated with a low-[Ca^{2+}] preactivating solution for 3 min. The preactivating solution was weakly buffered for Ca^{2+}, allowing rapid activation and force development upon introduction of the high-[Ca^{2+}] activating solution (18). Rapid, uniform activation of fibers in this manner ensured that the activation process itself did not introduce L_s nonuniformity.

Solutions

The skinning solution was composed of (mM): K-propionate, 125; imidazole, 20; EGTA, 5; $MgCl_2$, 2; ATP, 2; pH 7.0. The storage solution was composed of (mM): K-propionate, 125; imidazole, 20; EGTA, 5; $MgCl_2$, 2; ATP, 2; glycerol, 50% (v/v); pH 7.0. The relaxing solution (pCa ~9.0) was composed of (mM): HEPES, 90; Mg (total), 10.3; Mg^{2+}, 1.0; EGTA, 50; ATP, 8.0; CrP, 10.0; NaN_3, 1.0; Na (total), 36; K (total), 125; pH 7.1. The preactivating solution was composed of (mM): HEPES, 90; Mg (total), 8.50; Mg^{2+}, 1.0; EGTA, 0.10; HDTA, 50; ATP, 8.0; CrP, 10.0; NaN_3, 1.0; Na (total), 36; K (total), 125; pH 7.1. The activating solution (pCa ~4.5) contained (mM): HEPES, 90; Mg (total), 8.12; Mg^{2+}, 1.0; EGTA, 50; Ca^{2+} (total), 50; ATP, 8.0; CrP, 10.0; NaN_3, 1.0; Na (total), 36; K (total), 125; pH 7.1.

Determination of fiber CSA

After L_s was adjusted to ~2.5 μm, each fiber was imaged digitally from above and then from the side using a prism embedded in the chamber wall. Pairs of diameters were measured, one from each image, at five equally spaced locations along the midsection of the fiber using custom image-analysis software developed in MATLAB (The MathWorks, Natick, MA). The CSA was calculated for each of the five locations based on the assumption that the cross section of the fiber was elliptical. The fiber CSA was calculated as the mean of the five individual measurements.

L_s measurements

The hypothesis that during lengthening of a maximally activated fiber, regions that contain longer sarcomeres undergo more stretch than regions that contain shorter sarcomeres was tested by rapid measurement of the sarcomere lengths of each of 20 contiguous spots along the fiber (hereafter referred to as ''sectors'') before and at the peak of the stretch. Laser diffraction was selected to make the necessary high-speed sarcomere length measurements because the technique 1), has been used widely in previous investigations of L_s; 2), offers a superior signal/noise ratio and a more complete utilization of the dynamic range of the detectors compared with direct optical imaging (19–22); 3), requires minimal optics and consequently minimizes the effects of aberrations that pose significant challenges in optical imaging techniques; and 4), utilizes inexpensive light sources and optical-to-electrical conversion systems. To test our hypothesis, a major modification was made in the measurement methodology of laser diffraction from a traditional single-point measurement to a multiple-point measurement requiring rapid translation of the laser beam along the fiber.

L_s measurements were made from the diffraction patterns that resulted from transillumination of a small volume of the fiber with a laser beam having an e^{-2} beam width of ~180 μm (based on Gaussian intensity distribution, ~66% of the laser intensity was concentrated in the central 90 μm; ~35 sarcomeres in series). A diode laser operating at a wavelength of 650 nm was used. Translation of the laser spot was accomplished with a slow shear wave TeO_2 acousto-optic beam deflector (AOBD, model N45070-6; NEOS Technologies, Melbourne, FL driven by a digital radio frequency synthesizer oscillator (model N640410-200-2ASDFS; NEOS Technologies). The AOBD was located ~60 cm from the fiber so that the maximum laser beam deflection required to interrogate the full length of the fiber was <2 mrad. This ensured that angle effects on the diffraction peak intensity (23) were minimized. The resulting diffraction patterns were captured with a 2048-element charge-coupled device linear array sensor (model LD3543PGK; Perkin Elmer Optoelectronics, Fremont, CA) and a frame grabber (model PCI-1428; National Instruments, Austin, TX). A complete interrogation of the length of the fiber segment (L_{op}) was accomplished by translating the laser beam through the 20 sectors and scanning the diffraction pattern that was produced on the sensor by each sector. A complete readout from the sensor (referred to as a ''scan'') was a sequence of 2048 unsigned 8-bit integers that represented the intensity profile of the diffraction pattern. At each sector on the fiber, the laser spot was locked for 100 μs and one scan of the diffraction pattern was acquired. Thus the time taken to complete one full cycle of 20 scans (hereafter referred to as a ''sweep'') was 2 ms. For a given contraction protocol, servomotor and AOBD command arrays were precalculated and stored in the computer. Command arrays were updated to the respective instruments at a rate of 10 k updates s^{-1}. All inputs and outputs were gated by a single trigger pulse generated simultaneously on several trigger lines on a real-time system integration bus. The diffraction, servomotor, and force data were captured simultaneously at 10 k s^{-1} and stored by computer. A custom LabVIEW (National Instruments) program controlled the instruments and acquired and saved the data.

The diffraction data from one full sweep of a fiber (a matrix of 20 × 2048 elements) is shown in Fig. 2 *A* as a grayscale image. Each scan was preprocessed with a low-pass filter and folded along the centroid of the undiffracted (zero-order, 0°) intensity profile (Fig. 2). The intensity profiles of the two first-order profiles (−1° and +1°), thus falling on each other, were averaged to obtain the mean first-order (1°) profile. At any time point, L_s for a given sector was calculated based on the distance between the peak locations of 0° and 1° profiles by using the standard grating equation, $\lambda = L_s \cdot \sin\theta$, where θ is the diffraction angle between the 0° and the diffracted (1°) beams, and λ is the wavelength of the laser. Both the −1° and +1° orders were used (by obtaining 1°) in the L_s calculation to minimize volume diffraction effects (23–26). The 1° peak locations were estimated using the centroid method (27) given in the following equation:

$$\hat{p} = \frac{\sum_{p} I(p) \times p}{\sum_{p} I(p)}, \quad (1)$$

where, $I(p)$ is intensity at pixel p, and $\hat{p}$ is the centroid of the sequence I.

Sweeping

Sweeping was accomplished by generating a stair-step waveform of total amplitude proportional to the length of the sweep, and then using the stair-step waveform as the input to the radio frequency driver of the AOBD to translate the laser beam along the fiber in equally spaced steps (Fig. 3). When the length of the fiber was changed, the intervals were adjusted proportionally to ensure that the entire L_{op} was interrogated. The stair-step waveforms were precalculated for a given fiber length change protocol and stored in the computer.

Experimental protocol

The mean resting L_s was set to ~2.7 μm before the fiber was activated because the mean L_s within L_{op} shortens up to 6% during the isometric activation phase before the stretch. The resting L_s value was chosen to ensure that the stretch of an activated fiber was initiated with mean L_s in the middle of the plateau region or early part of the descending limb (28,29) of the length-tension relationship (see Discussion). An activated fiber was then lengthened by a single stretch of magnitude 0.27 L_f. The velocity of the stretch was 0.54 L_f s^{-1} (Fig. 4 *A*). After the stretch, the fiber was returned to its original length at the same velocity. Immediately upon return to the original length, the fiber was shortened rapidly (within 1 ms) by a length of 0.22 L_f and held for 40 ms. The fiber was then returned rapidly (within 1 ms) to its original length and allowed to generate maximum isometric force (Fig. 4). The rapid shortening-return maneuver was performed to establish the true zero of the force transducer. A typical force response of a fiber to the single stretch protocol is shown in Fig. 4 *B*.

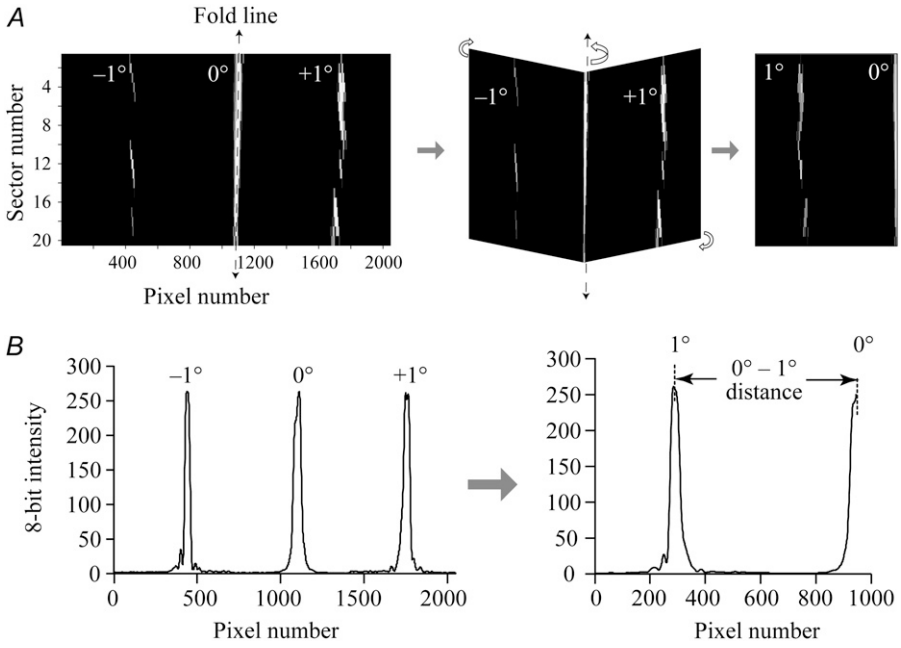

FIGURE 2 Method to determine the diffraction angle. (*A*) Scheme to obtain the 1° diffraction patterns from the −1° and +1°. The grayscale map (*left*) represents the diffraction data (all 20 scans) from a full sweep of the fiber. The *x* axis of the map represents the pixel number, and the *y* axis the sector number. The grayscale intensity of the image is proportional to the 8-bit intensity of the diffraction patterns (black 0 to white 255). The dashed line represents the fold line obtained by fitting a straight line to the centroids of the intensity profiles of the undiffracted order (0°). (*B*) A typical 8-bit intensity profile (*left*) of the diffraction pattern corresponding to sector 10 of the grayscale map. The intensity on the *y* axis is in arbitrary units (0−255). The intensity profile in the right panel corresponds to the 1° and left half of the 0°. The distance between the 1° and 0° peak locations (separation in pixels × the pixel size) and the fiber-to-sensor distance were used to compute the diffraction angle.

Force deficit measurements

Force deficit (10), the percentage reduction in maximum isometric force (P_o) after the stretch of an activated fiber, was calculated from the isometric force generated by a maximally activated single fiber before and after the single stretch protocol. Post-stretch force was measured twice: once during the first activation after a fiber was returned to its original length (Fig. 4) and once during a subsequent isometric activation, 15 min after the lengthening contraction. The difference between the two post-stretch isometric force measurements was <5% for all fibers used in this study, and the force deficit was calculated as their mean.

Compliant end-sectors

In permeabilized single-fiber preparations, some of the sectors adjacent to the points at which the fiber is secured to the apparatus lengthen substantially during maximum isometric activation due to the increased compliance of weaker sarcomeres that have been compromised by the attachment (30–34). Visual inspection of the fiber preparations showed a distinct change in the aspect ratio of the fiber near the ends (19), resulting in curved fiber boundaries. As myofibrils in the sectors adjacent to the attachment points pass through the curved boundaries, their axes are no longer parallel to the fiber axis. Consequently, for those myofibrils, the component of the tension vector that is

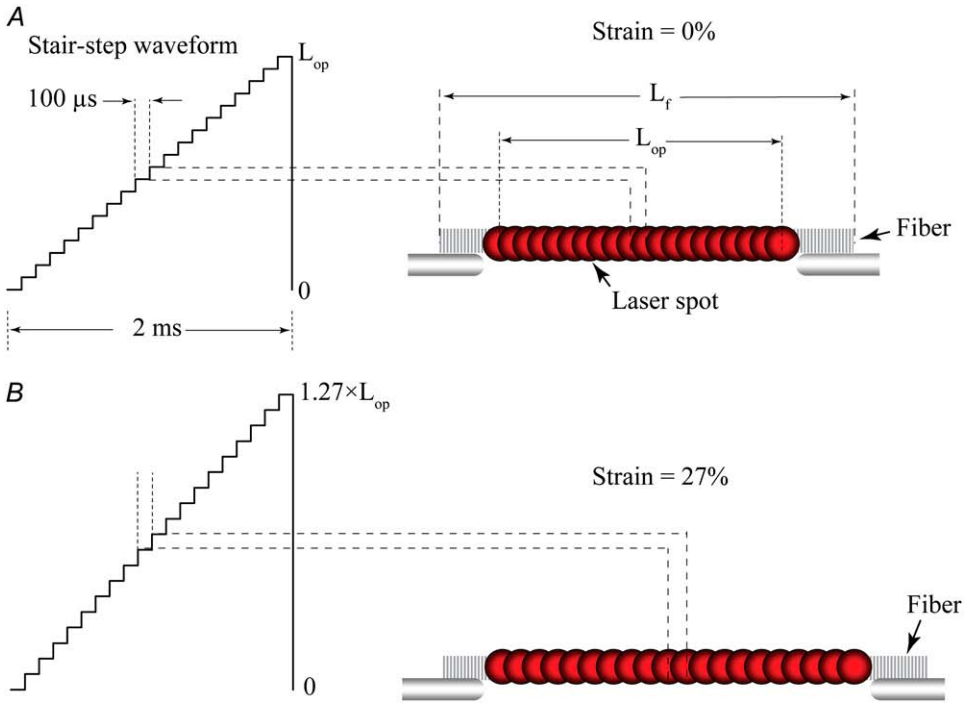

FIGURE 3 Translation of the laser beam during a sweep. (*A*) A typical stair-step waveform (*left*) representing one complete sweep. The step height corresponds to the separation distance between the centers of two adjacent sectors, and the step width corresponds to the duration of time that the laser spot was locked at the sector. An illustration of the sweeping with overlapping laser spots for an unstretched fiber is shown on the right. (*B*) When fiber length was increased, the separation between the adjacent laser spots was increased such that the entire L_{op} span continued to be interrogated.

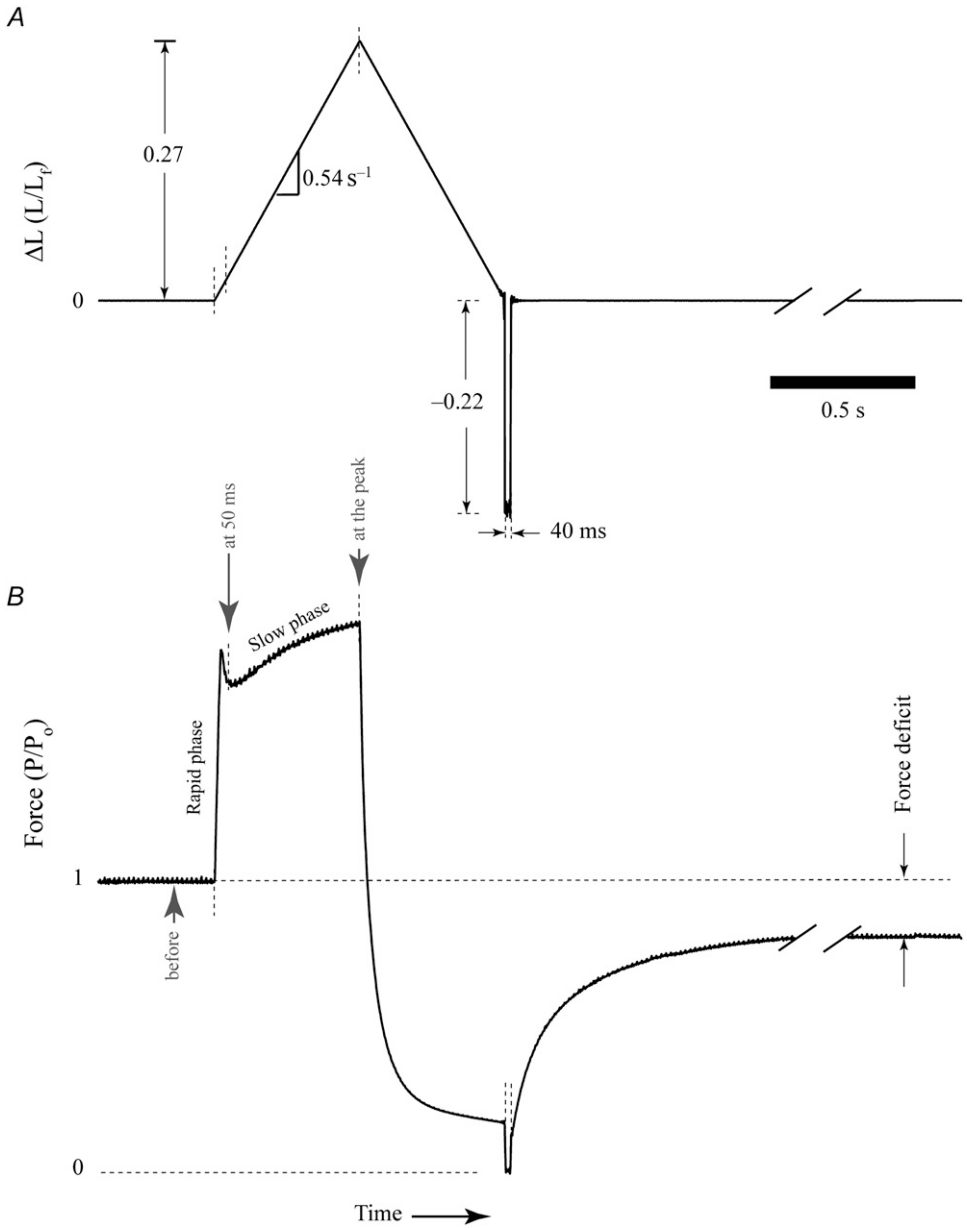

FIGURE 4 Experimental protocol. (*A*) Change in fiber length during the single stretch lengthening contraction protocol. Activated fibers were subjected to 27% stretch followed by shortening at constant speed. Immediately after the fibers were returned to original length, a step-shortening and stretch maneuver was inserted to indicate the zero of the force transducer on the force record. (*B*) A typical force response of the fiber to the single stretch protocol on the same timescale as shown in panel *A*. The force response of the fiber to stretch consisted of an initial phase of rapid increase followed by a phase of slow increase. The zero of the force transducer was established during the 40 ms hold after the step-shortening of the fiber. After the stretch, steady-state isometric stress was reassessed and used in force deficit calculations.

parallel to the fiber axis is less than that of the myofibrils in other sectors where the fiber aspect ratio is preserved. The change in aspect ratio is also likely to indicate an altered myofilament lattice, which will also contribute to a reduced generation of tension in those sectors. Due to this increased compliance at the ends, fully functional sectors in the middle of the fiber shorten at the expense of the end sectors, causing the end sectors to lengthen. Our data indicate that during maximal activation, the lengthening of sarcomeres near the attachment points can extend as far as 200 μm toward the fiber mid-point. Furthermore, the change in L_s from subfunctional sectors to functional sectors, as shown by our data (Fig. 5), is gradual. Consequently, the simple criterion of either shortening or lengthening of sectors during a maximal activation is not sufficient to identify the boundary between functional and subfunctional sectors. Instead, the curvature of the relationship between sector position and L_s is a better indicator of this boundary. Compliant sectors at the ends of the fiber were thus identified using a rate-limiting filter, and those sectors were eliminated from subsequent analyses (Fig. 5). The algorithm for the rate-limiting filter assumed that the middle 10 sectors of the fiber were not affected by attachment artifacts. The inclusion criterion for a new sector R on the right half of the fiber (sector numbers 16−20) was as follows: L_s of R must be less than L_s of $R - 1 + 1/2 \times$ SD of L_s of all the previously included sectors. The algorithm continued to the right only if sector R met the inclusion criterion. Similarly, when sectors in the left half of the fiber (sector numbers 5−1) were analyzed, sector R was included only if L_s of R was less than L_s of $R + 1 + 1/2 \times$ SD of L_s of all the previously included sectors. The algorithm proceeded to the left only if sector R met the inclusion criterion. Sector selection within one-half of the fiber was carried out independently from the other half, and the final set of sectors included for analysis was obtained by the union of the two halves.

A comparative study by Hilber and Galler (34) on the reliability of experiments using permeabilized single fibers with and without glutaraldehyde fixation of the fiber ends showed that results were comparable for the two preparation types only when the experimental duration was short. Fixing the ends with glutaraldehyde improved the reliability and stability of the experiments that involved longer periods of activation. The activation times in our experimental protocols were ~20 s, much less than the periods of 3−30 min reported in the study of Hilber and Galler (34). The short activation

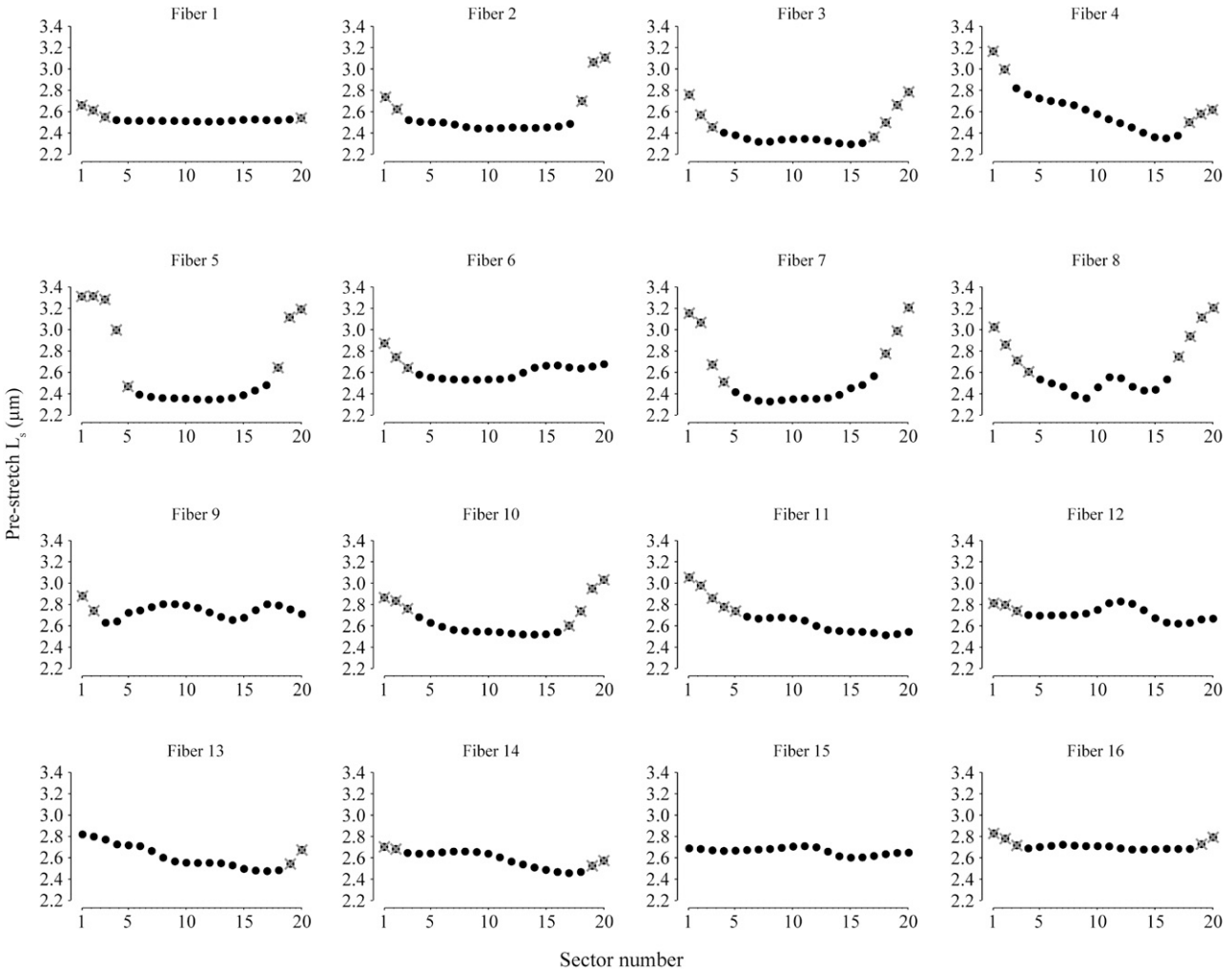

FIGURE 5 Sector exclusion map. Each panel shows the effect of the rate-limiting filter on the prestretch L_s profile of each of the 16 fibers. Note the increasing trend in prestretch L_s near the end-sectors. The sectors that were eliminated (*solid circles* with *crosses* through them) and those that were not eliminated (*solid circles*) with the rate-limiting filter are indicated on each L_s profile.

times, coupled with our acceptance criteria based on visual inspection of the quality of the laser diffraction patterns and elimination of excessively compliant end-sectors, ensured that the stability of the preparations used in the study presented here was not an issue.

Statistical analysis

To determine differences between relative stretch magnitudes at different prestretch L_s values, the relative stretch magnitudes of sectors were grouped according to the prestretch L_s of the sector (see Fig. 8), and then group means were assessed by a univariate one-way analysis of variance (ANOVA). If the F-statistic of the ANOVA showed significance, the differences were determined by Tukey's HSD post hoc tests for multiple comparisons. The level of significance was set a priori at $p < 0.05$. Pearson's product moment (r, correlation coefficient) was used to determine the correlation between prestretch L_s and stretch magnitude (Fig. 6 *B*), and relative prestretch L_s and relative stretch magnitude (Fig. 7).

RESULTS

The lengths of the fibers were $L_f = 1.37 \pm 0.14$ (mean $\pm$ SD, $n = 16$) and $L_{op} = 1.05 \pm 0.11$ mm. The CSA was 6490 $\pm$ 1410 μm^2, P_o was 0.86 $\pm$ 0.17 mN, stress was 135 $\pm$ 25 kN m^{-2}, and the force deficit after the lengthening contraction was 19% $\pm$ 9% P_o. For each fiber, the L_s for all sectors was computed from the diffraction patterns captured just before the stretch, 50 ms after the onset of the stretch, and at the peak of the stretch. The rate-limiting filter described in Materials and Methods was applied to the prestretch L_s profile to identify the functional sectors (Fig. 5). Of 320 sectors from the 16 fibers, 245 functional sectors were identified for further analyses. The responses of the remaining 75 sectors were excluded from the analyses and are not represented in the results shown in Figs. 6–8. The number of sectors retained for analyses varied among fibers (range = 11−20 sectors). For the accepted sectors of each fiber, we computed 1), the mean prestretch L_s; 2), the increase in L_s for each sector 50 ms after the beginning of the stretch and 3), at the peak of the stretch; and 4), the mean increase in L_s for all sectors 50 ms after the beginning of the stretch and 5), at the peak of the stretch. We chose to assess L_s behavior 50 ms after the initi-

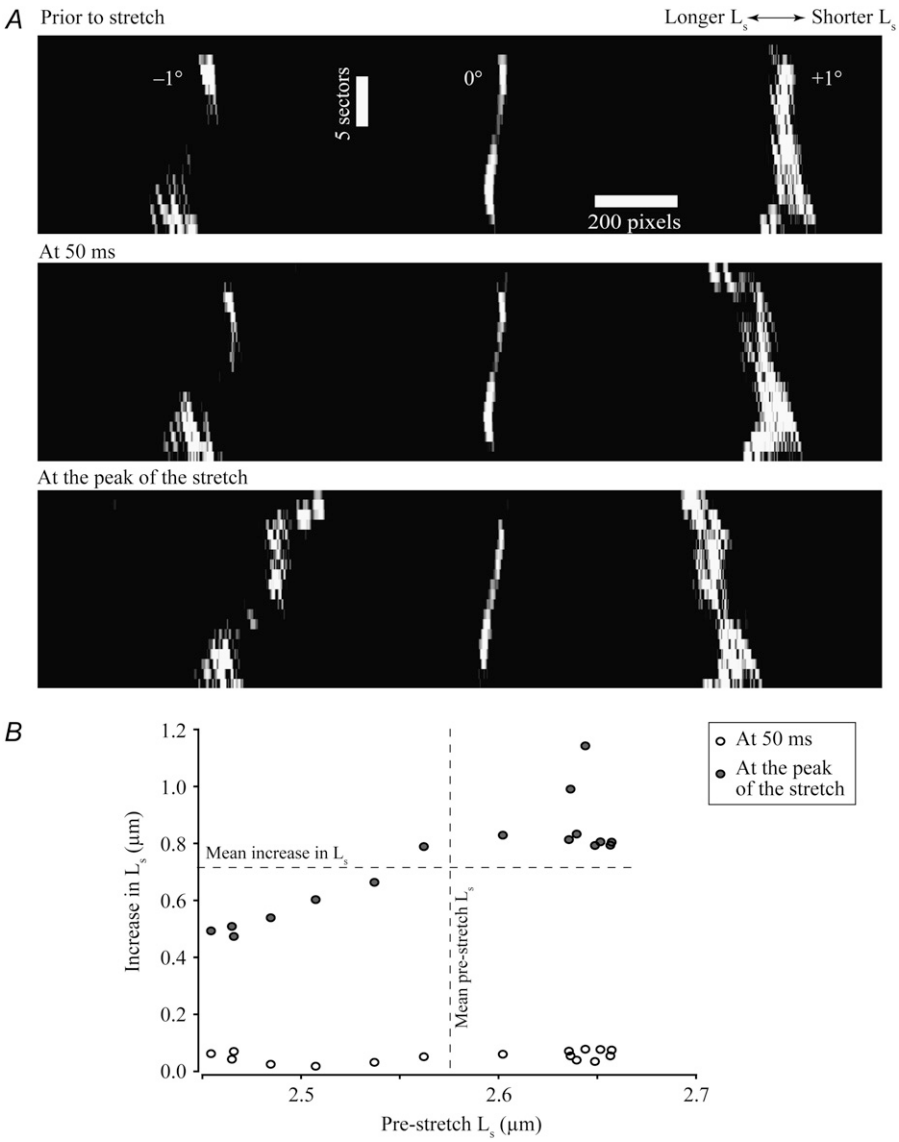

FIGURE 6 Representative diffraction images and L_s of an activated fiber (*Fiber 12*, Fig. 5) during the single stretch protocol. (*A*) L_s were computed from the diffraction images of the activated fibers obtained 100 ms before (*top*), 50 ms after the onset (*middle*), and at the peak of the stretch (*bottom*). Functional sectors were identified by applying the rate-limiting filter to the prestretch L_s, obtained from the top image. (*B*) For the accepted sectors, the increases in L_s during the stretch are plotted against the prestretch L_s. The graph shows a strong correlation ($r = 0.86$, $p < 0.0001$) between the increase in L_s at the peak of the stretch (*shaded circles*) and prestretch L_s, and indicates that sectors with prestretch L_s longer than the mean L_s stretched more than the mean increase in L_s (top-right quadrant). No such correlation was evident 50 ms after the onset of the stretch (*open circles*).

ation of the stretch on the basis that the increase in the force response changes from a rapid phase to a slow phase at this time. Frequently, a transient fall in force occurs during the transition from the rapid to the slow phases of the stretch (Fig. 4 *B*). The slow phase of the increase in force began after the fibers had absorbed ~2–3% strain. Based on data from all of the sectors included in the analyses, mean L_s values were computed for each fiber. The fiber-mean prestretch L_s ranged from 2.33 to 2.73 μm (mean = 2.54 ± 0.12 μm) and increased between 0.05 and 0.13 μm at 50 ms after the onset of the stretch and between 0.37 and 0.83 μm at the peak of the stretch.

In general, a nonuniform distribution of the stretch was observed along activated fibers, a finding consistent with previous reports (17,35–37). Representative diffraction patterns of an activated fiber before the stretch, at 50 ms after the onset of the stretch, and at the peak of the stretch are shown in Fig. 6 *A*. For the same fiber, the increase in L_s for each sector is plotted relative to its prestretch L_s in Fig. 6 *B* and shows that prestretch L_s did not appear to influence the increase in L_s at 50 ms. In contrast, at the peak of the stretch the sectors with prestretch L_s longer than the mean L_s underwent a greater increase in L_s than the mean (top-right quadrant). Similarly, sectors with shorter prestretch L_s underwent a smaller increase in L_s than the mean at the peak of the stretch (bottom-left quadrant).

For each sector in a given fiber, L_s was divided by the mean of the L_s values for all accepted sectors within that fiber and the ratio was termed the relative prestretch L_s (Fig. 7, *horizontal axes*). Similarly, the relative increase in L_s of a sector at 50 ms was calculated as the ratio of the increase in sector L_s after the first 50 ms of the stretch to the mean increase after 50 ms. The relationship between the relative prestretch L_s and the relative increase in L_s of a sector at 50 ms is shown in Fig. 7 *A*. The figure was obtained by pooling the data from all sectors of the 16 fibers (245 data points). The graph indicates that rela-

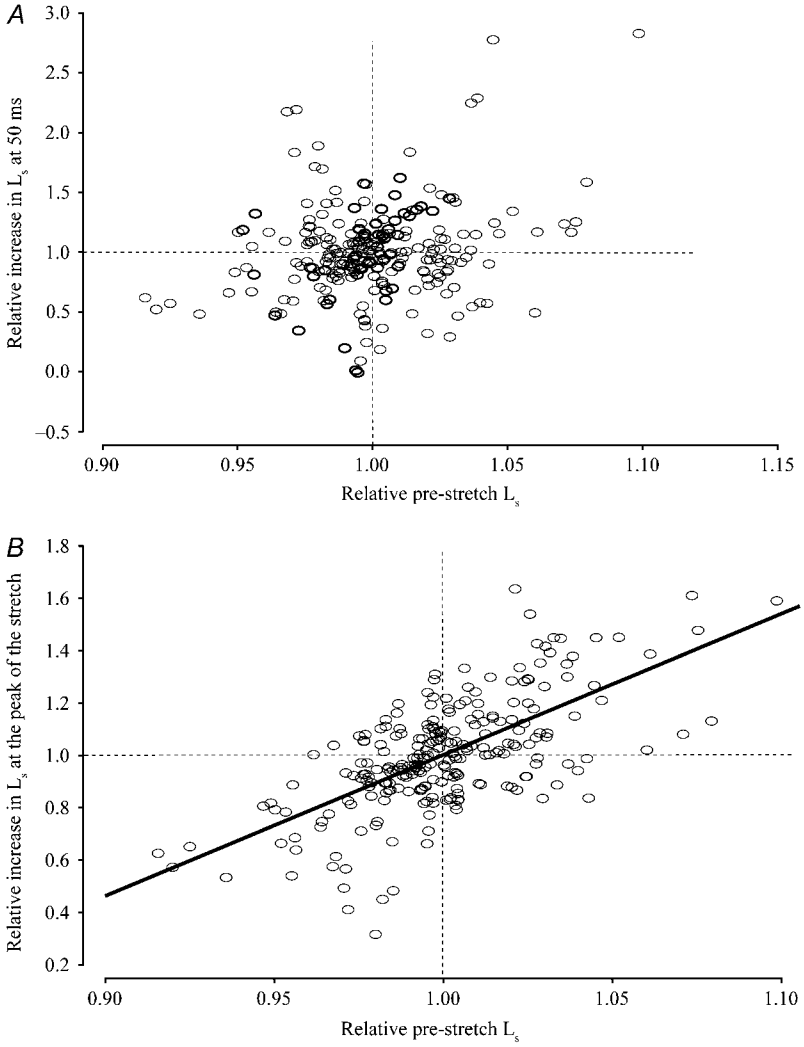

FIGURE 7 Effect of relative prestretch L_s on extensibility of sectors during stretch. The x axes represent relative prestretch L_s, the ratio of sector prestretch L_s to the mean L_s of the accepted sectors within a given fiber. (*A*) The y axis represents the relative increase in L_s 50 ms after the onset of the stretch (the ratio of the increase in sector L_s at 50 ms to the mean L_s increase at 50 ms). The relative increase in L_s did not correlate with relative prestretch L_s ($r = 0.23$, $p = 0.0003$). (*B*) The y axis represents the relative increase in L_s at the peak of the stretch (the ratio of the increase in sector L_s at the peak of the stretch to the mean L_s increase at the peak of the stretch). The relative increase in L_s correlated positively with the relative prestretch L_s ($r = 0.65$, $p < 0.0001$, slope = 5.4). The graph indicates that sectors with prestretch L_s longer than the mean of all accepted sectors within a given fiber extend more than the mean extension, and that sectors with shorter prestretch L_s than the mean extend less than the mean.

tive prestretch L_s and relative increase in L_s at 50 ms did not correlate. The relationship between relative prestretch L_s and relative increase in L_s at the peak of the stretch is plotted in Fig. 7 *B*. In contrast to the lack of correlation at 50 ms, the relative increase in L_s at the peak of the stretch was positively correlated with relative prestretch L_s. The graph (Fig. 7 *B*) indicates that if a sector was initially at a L_s longer than the mean (indicated by the *broken vertical line*), then during the stretch that sector was extended more than the mean (indicated by the *broken horizontal line*). Such sectors fall into the top-right quadrant of the graph. Similarly, the sectors in the bottom-left quadrant began with shorter prestretch L_s and stretched less than the mean stretch. A comparison of the graph in Fig. 7 *A* with the graph in Fig. 7 *B* indicates that this relationship was established during the slow phase of the rise in tension, not during the rapid phase (Fig. 4 *B*). It should also be noted that the L_s of all sectors in this study increased during the lengthening contraction (38), including those with the shortest prestretch L_s (Fig. 7 *B*).

To further analyze the effect of the prestretch L_s on the nonuniform increase in L_s (Fig. 8), the relative increases in L_s at the peak of the stretch for all 245 sectors were assigned to one of six groups according to the prestretch L_s values. The groups were distributed equally over a range of 2.25−2.85 μm with an interval of size 0.1 μm, and the means and 95% confidence interval bars were plotted for the individual groups (Fig. 8). The group means correlated with the mid-interval value of the x axis ($r = 0.88$, $p = 0.02$). A one-way ANOVA of the group means resulted in a significant F-statistic ($F = 8.31$). The post hoc multiple comparisons of mean values among the groups showed significant differences (Fig. 8). These tests revealed a biphasic relationship between prestretch L_s and relative increase in L_s, with the increase in L_s being independent of prestretch L_s in the range of 2.25−2.60 μm followed by an increasing trend for values of prestretch L_s >2.60 μm. The prestretch L_s value at which the change in the trend of the relative increases in L_s occurred coincided approximately with the beginning of the descending limb of the length-tension relationship for soleus muscle fibers from rats (28,29) (Fig. 8). The confidence intervals indicated that the spread of data points in each group was substantial, but no systematic changes in the spread of data points with L_s were observed (Fig. 8).

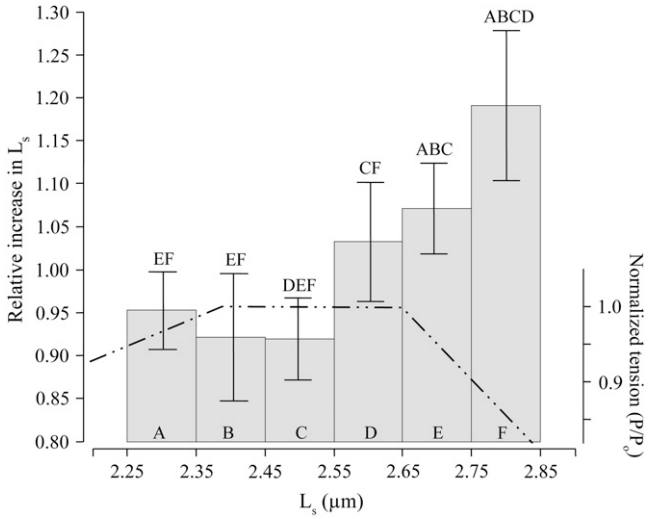

FIGURE 8 Relative increase in L_s at the peak of the stretch versus prestretch L_s. The data from all 16 fibers (245 sectors) were pooled and the relative increases in L_s of sectors were assigned to six different groups (A–F) according to the prestretch L_s values. The y axis on the left side of the graph represents the relative increase in L_s as a ratio of increase in L_s to mean increase in L_s for a given fiber, and the x axis represents the prestretch L_s of the sectors in μm. The groups were divided uniformly in the prestretch L_s range of 2.25–2.85 μm with an interval size of 0.1 μm. The group means and the error bars representing 95% confidence intervals for the means are shown in the figure. A one-way ANOVA to compare the group means resulted in a significant F-statistic ($F = 8.31$), indicating differences among groups. The post hoc comparisons identified pairwise differences ($p < 0.05$) as indicated above the bars of the histogram (e.g., group A is different from groups E and F). The L_s at which the shift in trend occurred coincided approximately with the beginning of the descending limb of the length-tension relationship (*dash-dotted line*, y axis on *right-hand side*) for the soleus muscles of rats.

DISCUSSION

Measurement of the behavior of sarcomeres

The testing of our hypothesis required major modifications of the current measurement methodology for laser diffraction from the traditional single-point to a multiple-point approach. Multiple-point monitoring of L_s behavior was introduced initially by Lieber et al. (39) for studies of intact single fibers from muscles of frogs. The single fiber performed multiple tetanic contractions and the fiber was translated axially through a stationary laser beam during the interval between the contractions. The system relied on the reproducibility of the behavior of L_s in a single fiber during repeated tetanic contractions. Such an approach is not applicable to investigations of the behavior of L_s during a protocol that causes an irreversible change in the behavior of sarcomeres. Macpherson et al. (17) translated a laser beam, before and after a single lengthening contraction, to five discrete locations along a stationary segment of a permeabilized single fiber in ~5 s to obtain spatially resolved data on L_s. The number of locations interrogated and time required for the measurements by Macpherson et al. (17) did not meet our requirements of high spatial and temporal resolution. We accomplished this by rapidly deflecting the laser beam through 20 serially connected sectors along the full length of the fiber segment in 2 ms. Although the diffraction pattern for each sector was acquired sequentially, the short duration of acquisition approximated an instantaneous ''snapshot'' of the sarcomere lengths along the full length of the fiber.

Complexity of sarcomere dynamics

The results indicated that L_s heterogeneity was present during a fixed-length contraction and that a stretch applied during the contraction was distributed nonuniformly along the fiber, increasing the heterogeneity. This uneven distribution of the stretch resulted in some mismatches between the position of the laser beam and the sarcomeres located within a given sector. As a consequence of this mismatch, a given sector number did not correspond exactly with the same population of sarcomeres from sweep to sweep. Analyses of the data indicated that such mismatches were of minor consequence; the magnitudes of all of the mismatches averaged 18% ± 9% for all of the sectors analyzed, and only 1% of the mismatches exceeded 50%. Furthermore, the spatial-frequency content of the L_s profiles before and at the peak of the stretch was very low (−3 dB frequency <0.07 cycles sector^{-1}), which made any errors introduced by either the contamination or loss of sarcomeres, for a given sector, insignificant. Although scanning with overlapping sectors resulted in some cross talk between sectors, the overlapping, rather than exclusion, was necessary to avoid undersampling and to obtain an accurate profile of the L_s of the entire fiber.

A few investigators (40,41) have used direct imaging of myofibrils to track individual sarcomeres or half-sarcomeres. Such an approach avoids cross talk between measurements of neighboring sarcomeres. Despite the absence of cross talk, the data obtained from a myofibril do not reflect the complex dynamics within a single fiber introduced by the lateral transmission of forces through the connections provided by cytoskeletal structures, such as desmin (42,43). The half-sarcomere (41) or sarcomeric (40) behavior within a single myofibril must be augmented by data supplied by numerical models to provide a realistic representation of fiber-level behavior (15). In contrast with the direct imaging methods, laser diffraction provides average information regarding the sarcomeres within a given sector, but the technique cannot resolve sarcomere-level events. Consequently, the application of the laser sweep technique to permeabilized single fibers provides data on sarcomere dynamics that complement those obtained from single myofibril imaging of single sarcomeres (40) or half-sarcomeres (16,41).

Nonuniformity of stretch along the fiber

In the study presented here, all lengthening contractions were preceded by a period during which the maximally activated fiber was maintained at a fixed length. The L_s nonuniformity

that was established during the fixed-length phase of the contraction served as the initial condition for the subsequent lengthening contraction and was assumed to be due to heterogeneity in the force-generating capabilities of the sectors. During the first 50 ms of the stretch of the maximally activated fiber, when the force was increasing rapidly, the increase in L_s of sectors did not appear to be influenced by their initial L_s. In contrast, during the slow phase of force increase, a systematic relationship developed between the prestretch L_s and the increase in L_s. The results indicated that, upon stretch of a maximally activated fiber, the increase in length was not distributed uniformly among the sectors of a fiber. Instead, sectors with longer prestretch L_s absorbed a relatively higher proportion of the stretch. The negative slope of the descending limb of the length-tension relationship has been implicated in the development of L_s nonuniformities at longer lengths (44,45). According to static-elastic theoretical models, sarcomeres that begin on, or are stretched onto, the descending limb during a contraction are weakened due to reduced opportunity for cross-bridge formation (13,46). As the lengthening contraction proceeds, the models predict a positive feedback cycle in which these weakened sarcomeres accept a disproportionately large fraction of the stretch, causing a further reduction in opportunity for cross-bridge formation, thereby exacerbating their weakness. Our results do not contradict this prediction.

Morgan (13) suggested that the positive feedback associated with lengthening on the descending limb of the length-tension relationship could cause the longest sarcomeres to undergo a rapid and uncontrolled lengthening (referred to as sarcomere ''popping'') until the force of the myofibril is borne completely by passive elements. The laser diffraction pattern that forms the basis for our measurements reflects the average length of the ~200,000 sarcomeres contained within a given sector of a single fiber. If sarcomere ''popping'' were to occur within single myofilaments, or even small groups of myofilaments, such sarcomere-level events would not be detected in the laser diffraction pattern of a fiber sector. Consequently, these results should not be interpreted as evidence supportive of the ''sarcomere popping'' hypothesis.

Relationship between strain and injury

A number of studies have shown a strong correlation between the magnitude of the strain of single fibers and the severity of injury as measured by the force deficit (7,10,47,48). This strain-dependence of injury, coupled with the finding of greater numbers of disrupted sarcomeres in permeabilized single fiber sectors with the longest prestretch L_s (17), implies that sectors with the longest prestretch L_s are those that are most strained during the subsequent lengthening contraction. Our study confirms that relationship. In a maximally activated fiber maintained at fixed length, groups of strong sarcomeres will shorten at the expense of the weaker sarcomeres, which will be stretched to longer lengths (49) and possibly onto the descending limb of the length-tension curve. A subsequent stretch of the fiber will place the long sarcomeres at a high risk of undergoing additional lengthening and damage as they absorb a higher proportion of the imposed stretch. A number of investigators have successfully identified focal injury to single or small groups of sarcomeres after a variety of protocols of single lengthening contractions (7,9,10,12,17,47,48,50), but a direct link between the injured sarcomeres and their lengthening behavior during the stretch has not been resolved. Our study, for the first time (to our knowledge), shows that in a maximally activated fiber the magnitude of the prestretch L_s is a good predictor of the magnitude of the relative increase in the L_s during a subsequent stretch. Coupled with the well-established relationship between strain and injury (7,10,47,48), this finding suggests that sectors with longer prestretch L_s are at higher risk of contraction-induced injury than those with shorter prestretch L_s. These data provide an explanation for the observation of Macpherson et al. (17) that, after a severe stretch, the regions of a fiber that were at longer sarcomere lengths during maximum activation before the stretch showed excessive damage to single sarcomeres and small groups of sarcomeres as viewed by electron microscopy after the stretch.

SUMMARY

We have developed a technique to measure spatially resolved L_s rapidly along the lengths of permeabilized single fibers, and demonstrated that stretches of maximally activated fibers are distributed nonuniformly along the fiber length. During a stretch of a maximally activated fiber, the increase in the nonuniformity of sarcomere lengths that developed during the stretch was due to sectors composed of the sarcomeres at longer lengths being stretched more than the sectors composed of sarcomeres at shorter lengths. These results support the hypothesis that the injury observed in individual sarcomeres, or small groups of sarcomeres, within single muscle fibers in a skeletal muscle that has undergone a severe lengthening contraction involves those sarcomeres or groups of sarcomeres that were at longer lengths when fibers were first activated. When such a muscle is activated and then lengthened, the single sarcomeres or groups of sarcomeres that are at longer lengths compared to their serially connected neighbors are at risk of being stretched excessively beyond the capability of the internal structure of the sarcomere to maintain its structural integrity.

REFERENCES

1. Faulkner, J. A. 2003. Terminology for contractions of muscles during shortening, while isometric, and during lengthening. *J. Appl. Physiol.* 95:455–459.
2. McCully, K. K., and J. A. Faulkner. 1985. Injury to skeletal muscle fibers of mice following lengthening contractions. *J. Appl. Physiol.* 59:119–126.

3. Friden, J., M. Sjostrom, and B. Ekblom. 1983. Myofibrillar damage following intense eccentric exercise in man. *Int. J. Sports Med.* 4:170–176.
4. Newham, D. J., G. McPhail, K. R. Mills, and R. H. Edwards. 1983. Ultrastructural changes after concentric and eccentric contractions of human muscle. *J. Neurol. Sci.* 61:109–122.
5. Ogilvie, R. W., R. B. Armstrong, K. E. Baird, and C. L. Bottoms. 1988. Lesions in the rat soleus muscle following eccentrically biased exercise. *Am. J. Anat.* 182:335–346.
6. Wood, S. A., D. L. Morgan, and U. Proske. 1993. Effects of repeated eccentric contractions on structure and mechanical properties of toad sartorius muscle. *Am. J. Physiol.* 265:C792–C800.
7. Brooks, S. V., E. Zerba, and J. A. Faulkner. 1995. Injury to muscle fibres after single stretches of passive and maximally stimulated muscles in mice. *J. Physiol.* 488:459–469.
8. Talbot, J. A., and D. L. Morgan. 1998. The effects of stretch parameters on eccentric exercise-induced damage to toad skeletal muscle. *J. Muscle Res. Cell Motil.* 19:237–245.
9. Brown, L. M., and L. Hill. 1991. Some observations on variations in filament overlap in tetanized muscle fibres and fibres stretched during a tetanus, detected in the electron microscope after rapid fixation. *J. Muscle Res. Cell Motil.* 12:171–182.
10. Macpherson, P. C., M. A. Schork, and J. A. Faulkner. 1996. Contraction-induced injury to single fiber segments from fast and slow muscles of rats by single stretches. *Am. J. Physiol.* 271:C1438–C1446.
11. Hunter, K. D., and J. A. Faulkner. 1997. Pliometric contraction-induced injury of mouse skeletal muscle: effect of initial length. *J. Appl. Physiol.* 82:278–283.
12. Talbot, J. A., and D. L. Morgan. 1996. Quantitative analysis of sarcomere non-uniformities in active muscle following a stretch. *J. Muscle Res. Cell Motil.* 17:261–268.
13. Morgan, D. L. 1990. New insights into the behavior of muscle during active lengthening. *Biophys. J.* 57:209–221.
14. Telley, I. A., J. Denoth, and K. W. Ranatunga. 2003. Inter-sarcomere dynamics in muscle fibres. A neglected subject? *Adv. Exp. Med. Biol.* 538:481–500.
15. Telley, I. A., and J. Denoth. 2007. Sarcomere dynamics during muscular contraction and their implications to muscle function. *J. Muscle Res. Cell Motil.* 28:89–104.
16. Telley, I. A., R. Stehle, K. W. Ranatunga, G. Pfitzer, E. Stussi, and J. Denoth. 2006. Dynamic behaviour of half-sarcomeres during and after stretch in activated rabbit psoas myofibrils: sarcomere asymmetry but no 'sarcomere popping'. *J. Physiol.* 573:173–185.
17. Macpherson, P. C., R. G. Dennis, and J. A. Faulkner. 1997. Sarcomere dynamics and contraction-induced injury to maximally activated single muscle fibres from soleus muscles of rats. *J. Physiol.* 500:523–533.
18. Moisescu, D. G., and R. Thieleczek. 1978. Calcium and strontium concentration changes within skinned muscle preparations following a change in the external bathing solution. *J. Physiol.* 275:241–262.
19. Julian, F. J., and R. L. Moss. 1980. Sarcomere length-tension relations of frog skinned muscle fibres at lengths above the optimum. *J. Physiol.* 304:529–539.
20. Myers, J., R. Tirosh, R. C. Jacobson, and G. H. Pollack. 1982. Phase-locked loop measurement of sarcomere length with high time resolution. *IEEE Trans. Biomed. Eng.* 29:463–466.
21. Krueger, J. W., and A. Denton. 1992. High resolution measurement of striation patterns and sarcomere motions in cardiac muscle cells. *Biophys. J.* 61:129–144.
22. Roos, K. P., R. J. Baskin, R. L. Lieber, J. W. Cline, and P. J. Paolini. 1980. Digital data acquisition and analysis of striated muscle diffraction patterns with a direct memory access microprocessor system. *Rev. Sci. Instrum.* 51:762–767.
23. Rudel, R., and F. Zite-Ferenczy. 1980. Efficiency of light diffraction by cross-striated muscle fibers under stretch and during isometric contraction. *Biophys. J.* 30:507–516.
24. Rudel, R., and F. Zite-Ferenczy. 1979. Interpretation of light diffraction by cross-striated muscle as Bragg reflexion of light by the lattice of contractile proteins. *J. Physiol.* 290:317–330.
25. Rudel, R., and F. Zite-Ferenczy. 1979. Do laser diffraction studies on striated muscle indicate stepwise sarcomere shortening? *Nature.* 278: 573–575.
26. Goldman, Y. E., and R. M. Simmons. 1984. Control of sarcomere length in skinned muscle fibres of Rana temporaria during mechanical transients. *J. Physiol.* 350:497–518.
27. Kawai, M., and I. D. Kuntz. 1973. Optical diffraction studies of muscle fibers. *Biophys. J.* 13:857–876.
28. Stephenson, D. G., and D. A. Williams. 1982. Effects of sarcomere length on the force-pCa relation in fast- and slow-twitch skinned muscle fibres from the rat. *J. Physiol.* 333:637–653.
29. Close, R. I. 1972. Dynamic properties of mammalian skeletal muscles. *Physiol. Rev.* 52:129–197.
30. Brenner, B. 1993. Dynamic actin interaction of cross-bridges during force generation: implications for cross-bridge action in muscle. *Adv. Exp. Med. Biol.* 332:531–542.
31. Chase, P. B., and M. J. Kushmerick. 1988. Effects of pH on contraction of rabbit fast and slow skeletal muscle fibers. *Biophys. J.* 53:935–946.
32. Martyn, D. A., and A. M. Gordon. 1992. Force and stiffness in glycerinated rabbit psoas fibers. Effects of calcium and elevated phosphate. *J. Gen. Physiol.* 99:795–816.
33. Galler, S., and K. Hilber. 1994. Unloaded shortening of skinned mammalian skeletal muscle fibres: effects of the experimental approach and passive force. *J. Muscle Res. Cell Motil.* 15:400–412.
34. Hilber, K., and S. Galler. 1998. Improvement of the measurements on skinned muscle fibres by fixation of the fibre ends with glutaraldehyde. *J. Muscle Res. Cell Motil.* 19:365–372.
35. Julian, F. J., and D. L. Morgan. 1979. The effect on tension of non-uniform distribution of length changes applied to frog muscle fibres. *J. Physiol.* 293:379–392.
36. Lombardi, V., and G. Piazzesi. 1990. The contractile response during steady lengthening of stimulated frog muscle fibres. *J. Physiol.* 431: 141–171.
37. Panchangam, A., R. S. Witte, D. R. Claflin, M. O'Donnell, and J. A. Faulkner. 2006. A novel optical imaging system for investigating sarcomere dynamics in single skeletal muscle fibers. *Proc. SPIE* 6088: 1–11.
38. Edman, K. A., G. Elzinga, and M. I. Noble. 1982. Residual force enhancement after stretch of contracting frog single muscle fibers. *J. Gen. Physiol.* 80:769–784.
39. Lieber, R. L., K. P. Roos, B. A. Lubell, J. W. Cline, and R. J. Baskin. 1983. High-speed digital data acquisition of sarcomere length from isolated skeletal and cardiac muscle cells. *IEEE Trans. Biomed. Eng.* 30:50–57.
40. Rassier, D. E., W. Herzog, and G. H. Pollack. 2003. Dynamics of individual sarcomeres during and after stretch in activated single myofibrils. *Proc. Biol. Sci.* 270:1735–1740.
41. Telley, I. A., J. Denoth, E. Stussi, G. Pfitzer, and R. Stehle. 2006. Half-sarcomere dynamics in myofibrils during activation and relaxation studied by tracking fluorescent markers. *Biophys. J.* 90:514–530.
42. Boriek, A. M., Y. Capetanaki, W. Hwang, T. Officer, M. Badshah, J. Rodarte, and J. G. Tidball. 2001. Desmin integrates the three-dimensional mechanical properties of muscles. *Am. J. Physiol. Cell Physiol.* 280:C46–C52.
43. Monti, R. J., R. R. Roy, J. A. Hodgson, and V. R. Edgerton. 1999. Transmission of forces within mammalian skeletal muscles. *J. Biomech.* 32:371–380.
44. Gordon, A. M., A. F. Huxley, and F. J. Julian. 1966. The variation in isometric tension with sarcomere length in vertebrate muscle fibres. *J. Physiol.* 184:170–192.

45. Gordon, A. M., A. F. Huxley, and F. J. Julian. 1966. Tension development in highly stretched vertebrate muscle fibres. *J. Physiol.* 184:143–169.

46. Edman, K. A., and C. Reggiani. 1984. Redistribution of sarcomere length during isometric contraction of frog muscle fibres and its relation to tension creep. *J. Physiol.* 351:169–198.

47. Brooks, S. V., and J. A. Faulkner. 1996. The magnitude of the initial injury induced by stretches of maximally activated muscle fibres of mice and rats increases in old ages. *J. Physiol.* 497:573–580.

48. Lieber, R. L., and J. Friden. 1993. Muscle damage is not a function of muscle force but active muscle strain. *J. Appl. Physiol.* 74:520–526.

49. Julian, F. J., and D. L. Morgan. 1979. Intersarcomere dynamics during fixed-end tetanic contractions of frog muscle fibres. *J. Physiol.* 293: 365–378.

50. Butterfield, T. A., and W. Herzog. 2006. Effect of altering starting length and activation timing of muscle on fiber strain and muscle damage. *J. Appl. Physiol.* 100:1489–1498.